



Double-Walled Carbon Nanotube Electrodes for Electrochemical Sensing

N. Punbusayakul,^{a,b,*} S. Talapatra,^c L. Ci,^b W. Surareungchai,^a and P. M. Ajayan^b

^aSchool of Bioresources and Technology, King Mongkut's University of Technology Thonburi, Bangkoktuen 10150, Thailand

^bDepartment of Materials Science and Engineering, Rensselaer Polytechnic Institute, Troy, New York 12180, USA

^cDepartment of Physics, Southern Illinois University, Carbondale, Illinois 62901, USA

We report on the electrochemical properties of electrodes fabricated using spun fibers of purified double-walled nanotubes (DWNTs). These electrodes show reversible and faster electron-transfer kinetics in electrochemical reactions compared to multi-walled nanotubes (MWNTs) and standard glassy carbon electrodes (GCE). The detection capabilities of the DWNT electrodes for chemical species such as hydrogen peroxide, ascorbic acid (AA), and electroactive neurotransmitters such as dopamine are presented and compared with the detection abilities for these species using GCE and MWNT. These electrodes also show excellent selective sensing properties (with observed detection limits as low as 20 μM of DA in 1 mM of AA) and can be developed for active components in electrochemical sensors.

© 2007 The Electrochemical Society. [DOI: 10.1149/1.2709398] All rights reserved.

Manuscript submitted August 14, 2006; revised manuscript received December 19, 2006.
Available electronically February 22, 2007.

Carbon nanotubes (CNTs) have gained considerable attention due to their exceptional electronic, mechanical, and chemical properties.¹⁻⁶ They also possess several unique features such as the ability to carry large current densities, and they have fast electron-transfer kinetics when used as electrodes⁷⁻⁹ for electrochemical sensing applications. This has led to the investigations of the electrochemical properties of various types of CNTs structures.¹⁰⁻¹⁷ Further, electrodes fabricated using CNTs for electrochemical sensing have the added advantage of reduced reaction potential and minimum surface fouling effects⁹⁻¹² and therefore offer superior performance when used as an electrochemical sensors. As a result of the ease of production of aligned multiwalled nanotube (MWNT) bundles, initially the electrochemical properties of macroarchitecture MWNT electrodes were extensively studied.¹⁸⁻²¹ Very recently the electrochemical properties of an individual single-walled nanotube (SWNT) electrodes fabricated using nanolithography and their possible use as nanoelectrodes for electrochemical applications were demonstrated.²² Typically electrode fabrication using SWNTs is complicated and therefore puts limitations for developing them for viable devices for electrochemical sensing applications. Electrodes fabricated with large ensembles of MWNTs, although showing promising electrochemical properties, are unable to provide good selectivity. With the development of techniques for bulk production of double-walled nanotubes (DWNTs),^{23,24} having physical properties similar to those of SWNTs, the possibility of developing these for various applications is envisioned. In this article we report on the electrochemical properties and sensing capabilities of DWNT ropes. The DWNT electrodes show a very wide window of operating potential without significant water hydrolysis. The superior ability of these electrodes for detection of frequently used electrochemical species like hydrogen peroxide (HP), L-ascorbic acid (AA), and dopamine (DA) is demonstrated. The DWNT electrodes are also able to distinguish extremely low concentrations of DA in the pre-mixed solution of AA and DA, indicating excellent selective sensing capabilities.

Experimental

The DWNTs used in this study were grown by chemical vapor deposition using xylene and ferrocene as previously described by Wei and co-workers.²⁵ The as-grown DWNT film was purified by first oxidizing at 400 °C in the oven for 4 h and then dipping into

concentrated hydrochloric acid solution to remove the impurities (mainly the catalyst particles). After the acid treatment the DWNTs were rinsed with distilled water. This process leads to the formation of entangled nets of purified DWNT. A short strand of DWNT was gradually peeled out from the DWNT net. The strand was then passed in the vicinity of a flame in order to remove the water and at the same time was continuously pulled and spun. This leads to longer DWNT fibers with typical diameters of ~ 10 to 50 μm . Glassy carbon electrode used in our study (diameter of 3 mm, model CH1104) was purchased from CH Instruments, Inc.

Cyclic voltammetry (CV) and chronoamperometry experiments were performed using a PAR 273A potentiostat-galvanostat with the PowerSuite data acquisition software. The CV measurements were conducted in a 10 mM $\text{K}_3\text{Fe}(\text{CN})_6$ containing 0.1 M KCl solution using a conventional three-electrode system with Ag/AgCl and platinum wire as reference and counter electrode, respectively. Potassium ferricyanide(III) powder ($< 10 \mu\text{m}$, 99+%), potassium chloride (99.0–100.5%), AA (99+%), and HP (30 wt % solution in water) were purchased from Sigma-Aldrich, Inc., and 5-hydroxytryptamine hydrochloride was purchased from Fluka. All solutions were freshly prepared in distilled water before each experimentation cycle. The potential was cycled from 0.6 to -0.2 V at scan rates of 5, 10, 20, 50, 100, 200, and 500 mV s^{-1} . Chronoamperometry experiments were also performed in order to get an electrochemical active area of the electrodes with the initial potential of 0.6 V for 0.2 s and a final potential of -0.2 V for 5 s using the same solution as in the CV measurement.

For fabricating the electrodes, the DWNT fiber was placed on a flat glass substrate. One end of the fiber was then attached to an electrical lead using silver paste and the other end of the fiber was fixed with epoxy glue. This was done for handling ease of the electrode. The electrode assembly was then appropriately placed in an electrochemical testing cell containing the electrolyte. Figure 1a shows the schematics of the electrode and the measurement setup. In Fig. 1b and c electron microscope images of the spun fibers of DWNT are shown. A high-resolution transmission electron microscopy (HRTEM) image, clearly showing two walls of the nanotube, is shown in Fig. 1d. In Fig. 1e we have presented the data from Raman measurements on our samples. The Raman spectra from the pristine fiber show the structural features of DWNTs. The radial breathing mode (RBM) in the lower frequency range displays mainly two groups of the peak. Group 1 originates from the outer tube and group 2 the inner tube. The much lower intensity of the D band compared to the G band indicates the lower content of amorphous carbon and the higher crystallization of the DWNTs.

* Electrochemical Society Student Member.

^z E-mail: ausrpi@gmail.com

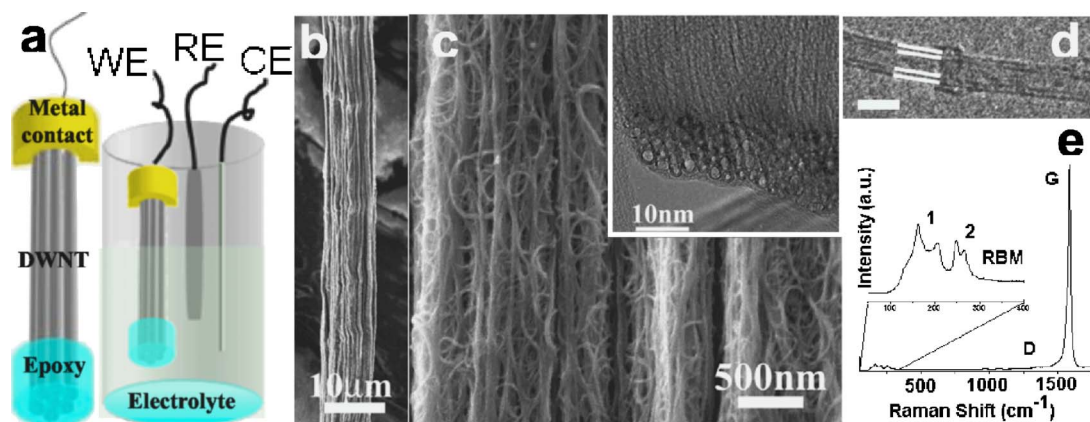


Figure 1. (a) (Color online) Schematics of the electrode fabricated using the DWNT and the experimental setup used for obtaining the CVs. WE, RE, and CE in the figure refer to the working electrode (DWNT fiber), the reference electrode (Ag/AgCl), and the counter electrode (platinum wire), respectively. (b) Scanning electron microscope image of a portion of the electrode. (c) A higher magnification view of the surface of a typical electrode showing the entangled bundles of DWNT. (Inset) An HRTEM image of single DWNT showing the two walls of the nanotube (scale bar is 3 nm). (e) Raman spectra of the DWNT samples used in our study.

Results and Discussion

In Fig. 2 the electrochemical characterization of the DWNT electrodes is presented. Figure 2a shows the CV of 0.1 M KCl obtained with a scan rate of 20 mV s^{-1} at the DWNT electrode. The absence of any peak in the voltammogram over a wide potential window (potential ranged from -1.4 to 1.2 V) signifies negligible water hydrolysis, a property which is extremely useful for determination of

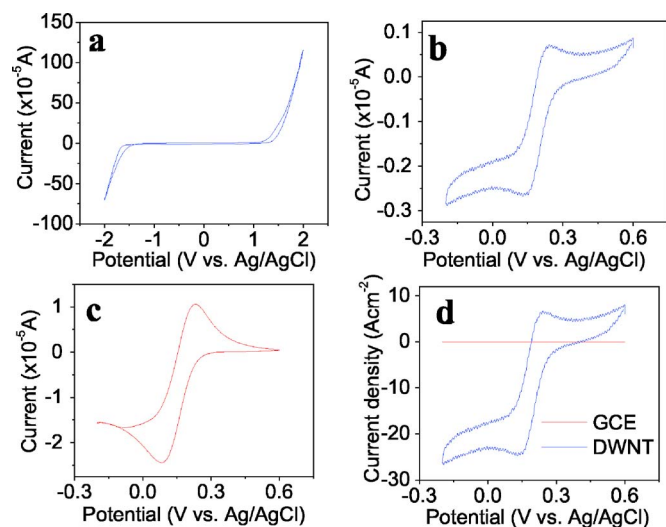


Figure 2. (Color online) CVs of (a) 0.1 M KCl at a scan rate of 20 mV s^{-1} at the DWNT electrode and of (b) $10 \text{ mM K}_3(\text{FeCN})_6$ containing 0.1 M KCl at a scan rate of 5 mV s^{-1} at (b) a DWNT electrode, (c) GCE, and (d) normalized (with active electrochemical area) current density at a DWNT electrode and GCE.

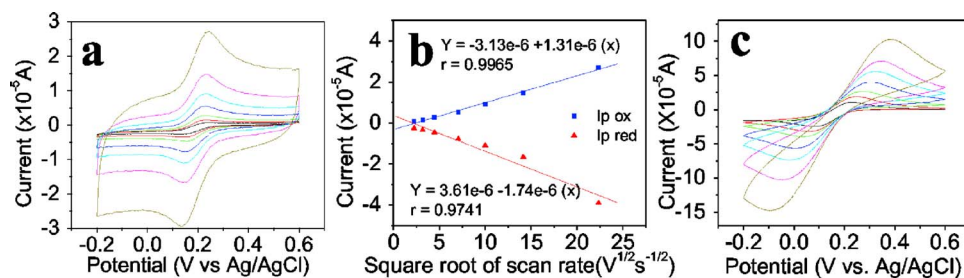


Figure 3. (Color online) (a) CVs of $10 \text{ mM K}_3(\text{FeCN})_6$ containing 0.1 M KCl at various scan rates: 5, 10, 20, 50, 100, 200, and 500 mV s^{-1} at the DWNT electrode (inner-to-outer loop, respectively). (b) Plot of the peak current vs the square root of the scan rate. Linear relationships were obtained for oxidation (■) and reduction (▲) peak current. (c) CVs obtained using GCE with the same condition as in (a).

chemical species having high oxidation and reduction peaks such as DA. In Fig. 2b and c CVs of $10 \text{ mM K}_3(\text{FeCN})_6$ containing 0.1 M KCl at a scan rate of 5 mV s^{-1} at a DWNT electrode and glassy carbon electrode (GCE), respectively, are shown. A very well-defined voltammogram with small double-layer capacitance was obtained at the DWNT electrode with the oxidation and reduction peak potential at about 235 and 146 mV, respectively.

The data presented in Fig. 2b and c was normalized with the electrochemical active areas of the respective electrodes and is shown in Fig. 2d. Chronoamperometry was used to determine the electrochemical active area of the electrodes based on the Cottrell equation,²⁶ $i_d = nFAD^{1/2}C^*\pi^{-1/2}t^{-1/2}(1)$, where i_d is the limiting current (A), n is the electron stoichiometry, A is the electrochemical active area of the electrode (cm^2), D is the diffusion coefficient of the $[\text{Fe}(\text{CN})_6]^{3-/4-}$ ($10^{-6} \text{ cm}^2 \text{ s}^{-1}$), C^* is the concentration of the interested species in bulk solution (mol L^{-1}), F is the Faraday's constant ($96,500 \text{ C mol}^{-1}$), and t is time (s). Note the higher current response of the DWNT compared to the GCE in Fig. 2d.

In Fig. 3 we show the voltammograms obtained at different scan rates for DWNT and GCE electrodes. Another feature that was observed from these voltammograms is that in the case of the DWNT electrodes there is negligible shift of the oxidation and reduction peaks, even at very high scan rates (500 mV s^{-1}) (Fig. 3a). Consequently, peak-to-peak separation potential (ΔE_p) for all scan rates is stable at $\sim 90 \text{ mV s}^{-1}$. This value is less than the ΔE_p values at some other nanotube electrodes previously reported on unmodified MWNT and SWNT electrodes,^{19-21,27,28} suggesting a faster electron-transfer rate at the DWNT electrode as compared to these electrodes. Moreover, we obtained linear dependence of the peak current as a function of the square root of the scan rate for these electrodes (Fig. 3b) using the Randles-Sevcik equation,²⁶ $I_p = 2.69 \times 10^5 n^{3/2}AD^{1/2}C^*v^{1/2}(2)$, where I_p is the peak current (A), n is the

Table I. Comparison of peak-to-peak separation potential (ΔE_p) and reaction type of various architectures of CNT and other carbon-based electrodes.

CNT	ΔE_p (mV)	Scan rate (mV/s)	Reaction ^a	References in main text
MWNT bundles	59	20–500	R	18
MWNT (heat-treated)	170	20	Q	19
MWNT film	146	100	Q	20
Long MWNT	75	100	Q	35
Nanoneedle MWNT	167	-	Q	36
SWNT	100	20	Q	19
SWNT (coated tungsten wires)	60	5–1000	R	27
SWNT paper (acid-treated)	74	5–500	R	28
SWNT-carbon fiber nanoelectrode	~150	10	Q-steady state	37
DWNT fibers	90	5–500	R	Present work

Carbon fiber (CF), diamond and carbon electrode	ΔE_p (mV)	Scan rate (mV/s)	Reaction ^a	References in main text
CF cone nanosize electrode	59	10–500	R-Steady state	38
CF ultramicroelectrode				39
Without any treatment	98	50	-	
Electrochemically pretreated	59			
Nitrogen-doped diamond-like carbon film	62	-	Q	40
Single-crystal diamond				
Without any treatment	-	-	Nonreversible	29
Electrochemical treatment	200	-	-	
300	300	100	Q	30
Doped diamond-coated CF diamond	180	10–500	Q	31
Polycrystalline diamond on graphite	510	100	Q	32
Doped-CVD diamond	261	100	Q	33
Boron-doped polycrystalline diamond				
Without any treatment	325	10	Q	34
Acid treatment	104	100	Q	

^a R indicates reversible; Q indicates quasi-reversible.

electron stoichiometry, A is the electrode area (cm^2), D is the diffusion coefficient of the interested species ($\text{cm}^2 \text{s}^{-1}$), C is the concentration of the species in the bulk solution (mol L^{-1}), and ν is the scan rate (V s^{-1}). The stable peak-to-peak separation potential and the linear plot indicate the diffusion-controlled and reversible reaction at the DWNT electrode. The negligible shift of the oxidation and reduction peaks (Fig. 3a) also suggests a fast electron-transfer rate at the DWNT electrode. On the contrary, a significant shift in the oxidation and reduction peaks was observed in the case of the GCE, as well as the aligned MWNT (for MWNT data is not shown) electrode. This shift results in the increasing peak-to-peak separation potential with increasing scan rates (Fig. 3c), suggesting slow electron-transfer rate as well as quasi-reversible reaction at the GCE. Similarly, the DWNT electrode is much better than previously studied diamond electrodes, since these electrodes have slower electron-transfer rates and sometimes need chemical modification or acid treatment in order to improve their electrochemical properties.^{29–34} A comparison between the various parameters characterizing the electrochemical properties of other carbon-based electrode materials is presented in Table I.

The uniqueness of the architecture used to make the electrodes is that it has a very high surface area because of parallel “strands” of DWNT. Further, the density of states of individual nanotubes can play a significant role in the efficiency and stability of the charge-transfer process when a nanotube is used as an electrode. Nanotubes with metallic density of states are expected to perform higher conductance, and hence are more efficient. When a large collection of nanotubes is collectively excited by an applied potential (as in the present case), the metallic tubes can selectively participate more

efficiently. In this respect, having a bundle of nanotubes is a better idea than a single tube which may or may not be metallic. The diameter of the individual tubes is also ~ 3 to 5 nm. Due to this small diameter, enhanced electric fields around the nanotube electrode are generated, which leads to the faster reaction rate as observed. We conjecture that a combination of the above properties of the DWNT nanotubes gives rise to the higher performances of the DWNT electrodes, as seen from our results.

The advanced electrochemical properties of the DWNT electrodes, as seen from CV measurements, make them suitable for sensitive, high-performance electrochemical sensor materials. For evaluating the electrochemical sensing abilities of this kind of electrode a series of model electroactive species (HP, AA, and DA) as analytes were chosen and tested. The results are shown in Fig. 4. As seen in Fig. 4a, the peak of the voltammogram is not seen for HP at both the GCE and the MWNT electrodes. This is due to the electrolysis of water, as also reported previously.^{41,42} However, greater response toward the oxidation of HP was obtained at the DWNT electrode than GCE. This implies that the DWNT electrode is significantly sensitive to the species and therefore is suitable for electroanalysis. In the case of AA the DWNT electrode gave the anodic peak of AA at ~ 552 mV, which is close to the peak potential as reported by Hu and co-workers⁴³ for a DNA-SWNT modified electrode and about 460 mV at a micrometer-size SWNT-coated tungsten wire.²⁸ Similarly, DA was found to be oxidized and reduced at the DWNT electrode at ~ 444 and 388 mV, respectively, which is consistent with the report of Mani and co-workers⁴⁴ for nanocrystalline graphite electrodes. However, this peak potential of DA at the DWNT electrode is higher than the redox potential observed on

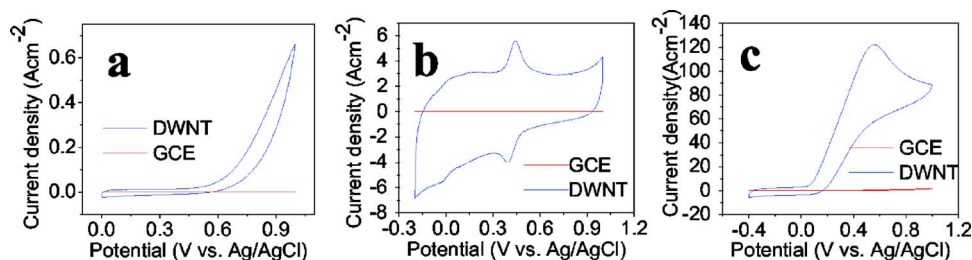


Figure 4. (Color online) CVs at the DWNT electrode in 0.1 mM of (a) HP, (b) DA, and (c) AA containing 0.1 M phosphate buffer solution pH 7.0 at a scan rate of 100 mV s⁻¹ showing the superimposed current response at the DWNT electrode over the GCE electrode for all tested species.

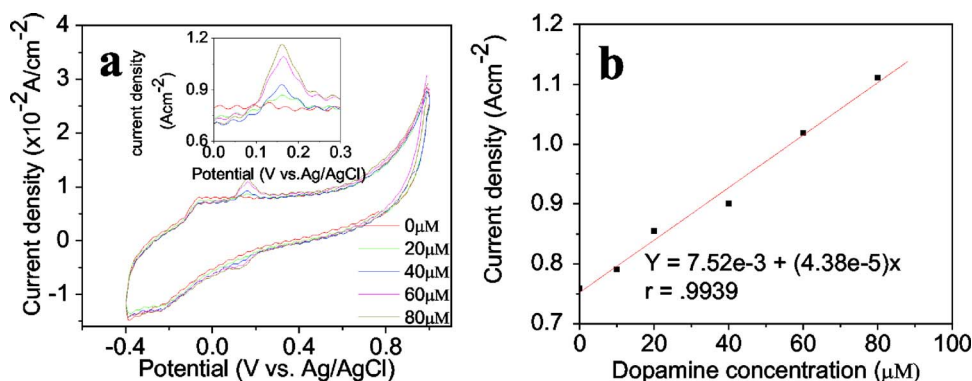


Figure 5. (Color online) (a) CVs at the DWNT electrode when AA concentration was fixed at 1 mM and the concentration of DA was varied from 10 to 80 μM. The oxidation peak of DA for each concentration is shown in the inset. (b) The variation of current density vs DA concentration.

SWNT-tungsten wire at the potential of 300 mV²⁷ and is higher than that of a DNA-SWNT modified electrode (220 mV),⁴³ probably due to the micrometer-size dimensions of the SWNT-tungsten wire electrode and the ability of overpotential reduction of DNA at the DNA-SWNT electrode.

These results indicate the possibility of efficient single-species detection capability of the DWNT electrodes for some of the chemicals which are important intermediates, main products, or by-products in various electrochemical analysis methods (for example, HP is the main analyte in glucose analysis, and AA is one of the most important compositions in foods). However, one of the major challenges in electrochemical sensing is to fabricate electrode materials which will have the ability to distinguish a particular species in a multicomponent mixture of various species. The issue of selective sensing becomes essential in the case of many real biological matrices containing two or more species. For example, AA is a major interference species of many biological reactions. This includes DA diagnostic tests also. The fact that the oxidation potential value of AA is very close to that of DA results in the overlap of these two peaks in a voltammogram⁴⁵ containing these two species. This poses severe restrictions in determination of DA concentrations, an important factor in diagnosis of diseases like Parkinson's. To demonstrate the selective sensing ability of the DWNT electrodes, we have performed CV experiments with varying concentrations of DA in a solution of AA and DA. The results are shown in Fig. 5.

Figure 5a shows CVs of the DWNT electrode with various concentrations of DA (10–80 μM) in 1 mM of AA. The oxidation peaks of AA and DA in this premixed solution were distinguishably observed at -70 and 168 mV, respectively, resulting in larger separating oxidation potential (230 mV) than previously reported at a DNA functionalized SWNT electrode.⁴³ We were able to distinguish AA and DA even at the very high scan rate of 100 mV s⁻¹. Our electrodes made of DWNT fibers were used without any complicated postproduction surface functionalization. We were able to determine DA for concentrations as low as 20 μM. In our experiments we found the current density to vary linearly with concentrations of DA up to 80 μM (Fig. 5b).

Conclusions

We have fabricated and determined the electrochemical properties of electrodes with DWNT fibers. The electrochemical sensing

tests indicate that this simple architecture of the DWNT electrodes can be used as effective electrochemical sensors for determining the presence of a variety of single species, as well as distinguishing multiple species of AA and DA which are often found in realistic biological environments.

Acknowledgments

N.P. thanks the Thailand Commission on Higher Education Fellowship. P.M.A. thanks the Nanoscale Science and Engineering Center for the directed assembly of nanostructures at RPI supported by the National Science Foundation. The authors thank Dr. S. Kar and Dr. R. Vajtai for helpful discussions.

King Mongkut's University of Technology Thonburi assisted in meeting the publication costs of this article.

References

- P. J. Britto, K. S. V. Santhanam, A. Rubio, J. A. Alonso, and P. M. Ajayan, *Adv. Mater. (Weinheim, Ger.)*, **11**, 154 (1999).
- R. H. Baughman, A. A. Zakhidov, and W. A. de Heer, *Science*, **297**, 787 (2002).
- J. J. Gooding, *Electrochim. Acta*, **50**, 3049 (2005).
- A. Merkoci, M. Pumera, X. Llopis, B. Perez, M. del Valle, and S. Alegret, *Trends Anal. Chem.*, **24**, 826 (2005).
- K. Gong, Y. Yan, M. Zhang, L. Su, S. Xiong, and L. Mao, *Anal. Sci.*, **21**, 1383 (2005).
- J. Wang, *Electroanalysis*, **17**, 7 (2005).
- J. K. Campbell, L. Sun, and R. M. Crooks, *J. Am. Chem. Soc.*, **121**, 3779 (1999).
- H. Cai, X. Cao, Y. Jiang, P. He, and Y. Fang, *Anal. Bioanal. Chem.*, **375**, 287 (2003).
- N. Zhang, J. Xie, and V. K. Varadan, *Smart Mater. Struct.*, **15**, 123 (2006).
- B. S. Sherigara, W. Kutner, and F. D. Souza, *Electroanalysis*, **15**, 753 (2003).
- D. Pan, J. Chen, S. Yao, W. Tao, and L. Nie, *Anal. Sci.*, **21**, 367 (2005).
- M. Pumera, A. Merkoci, and S. Alegret, *Sens. Actuators B*, **113**, 617 (2006).
- C. G. Hu, W. L. Wang, S. X. Wang, W. Zhu, and Y. Li, *Diamond Relat. Mater.*, **12**, 1295 (2003).
- J. Koehne, J. Li, A. M. Cassell, H. Chen, Q. Ye, H. Tee Ng, J. Han, and M. Meyyappan, *J. Mater. Chem.*, **14**, 676 (2004).
- M. Kaempgen and S. Roth, *Synth. Met.*, **152**, 353 (2005).
- C. E. Banks, T. J. Davies, G. G. Wildgoose, and R. G. Compton, *Chem. Commun. (Cambridge)*, **2005**, 829.
- Y. Tu, Y. Lin, W. Yantasee, and Z. Ren, *Electroanalysis*, **17**, 79 (2005).
- J. M. Nugent, K. S. V. Santhanam, A. Rubio, and P. M. Ajayan, *Nano Lett.*, **1**, 87 (2001).
- J. Li, A. Cassell, L. Delzeit, J. Han, and M. Meyyappan, *J. Phys. Chem. B*, **106**, 9299 (2002).
- R. R. Moore, C. E. Banks, and R. G. Compton, *Anal. Chem.*, **76**, 2677 (2004).
- C. Hu, Y. Zhang, G. Bao, Y. Zhang, M. Liu, and Z. L. Wang, *Chem. Phys. Lett.*, **418**, 524 (2005).

22. I. Heller, J. Kong, H. A. Heering, K. A. Williams, S. G. Lemay, and C. Dekker, *Nano Lett.*, **5**, 137 (2005).
23. Y. A. Kim, H. Muramatsu, T. Hayashi, M. Endo, M. Terrones, and M. S. Dresselhaus, *Chem. Phys. Lett.*, **398**, 87 (2004).
24. M. Endo, H. Muramatsu, T. Hayashi, Y. A. Kim, M. Terrones, and M. S. Dresselhaus, *Nature (London)*, **433** (2005).
25. J. Wei, B. Jiang, D. Wu, and B. Wei, *J. Phys. Chem. B*, **108**, 8844 (2004).
26. H. H. Girault, *Analytical and Physical Electrochemistry*, p. 304 and 379, EPFL Press, Italy (2004).
27. F. Valentini, S. Orlanducci, E. Tamburri, M. L. Terranova, A. Curulli, and G. Palleschi, *Electroanalysis*, **17**, 28 (2005).
28. F. Valentini, S. Orlanducci, M. L. Terranova, A. Amine, and G. Palleschi, *Sens. Actuators B*, **100**, 117 (2004).
29. T. Kondo, K. Hondo, D. A. Tryk, and A. Fujishima, *J. Electrochem. Soc.*, **152**, E18 (2005).
30. E. C. Almeida, A. V. Diniz, V. J. Trava-Airoldi, and N. G. Ferreira, *Thin Solid Films*, **485**, 241 (2005).
31. W. P. Kang, J. L. Davidson, Y. M. Wong, K. L. Soh, and Y. Gurbuz, *Proc.-IEEE Ultrason. Symp.*, **1**, 376 (2004).
32. R. Ramesham, *Thin Solid Films*, **339**, 82 (1999).
33. R. Ramesham and M. F. Rose, *Diamond Relat. Mater.*, **6**, 17 (1997).
34. G. M. Swain and R. Ramesham, *Anal. Chem.*, **65**, 345 (1993).
35. Y. Yun, V. Shanov, M. J. Schulz, Z. Dong, A. Jazieh, W. R. Heineman, H. B. Halsall, D. K. Y. Wong, A. Bange, Y. Tu, and S. Subramaniam, *Sens. Actuators B*, **120**, 298 (2006).
36. H. Boo, R. A. Jeong, S. Park, K. S. Kim, K. H. An, Y. H. Lee, J. H. Han, H. C. Kim, and T. D. Chung, *Anal. Chem.*, **78**, 617 (2006).
37. R. S. Chen, W. H. Huang, H. Tong, Z. L. Wang, and J. K. Cheng, *Anal. Chem.*, **75**, 6341 (2003).
38. X. Zhang, W. Zhang, X. Zhou, and B. Ogorevc, *Anal. Chem.*, **68**, 3338 (1996).
39. K. A. El-Nour and A. Brajter-Toth, *Electroanalysis*, **12**, 805 (2000).
40. A. Zeng, E. Liu, S. N. Tan, S. Zhang, and J. Gao, *Electroanalysis*, **14**, 1110 (2002).
41. M. Musameh, N. S. Lawrence, and J. Wang, *Electrochem. Commun.*, **7**, 14 (2005).
42. T. Hoshi, H. Saiki, S. Kuwazawa, C. Tsuchiya, Q. Chen, and J. I. Anzai, *Anal. Chem.*, **73**, 5310 (2001).
43. C. Hu, Y. Zhang, G. Bao, Y. Zhang, M. Liu, and Z. L. Wang, *J. Phys. Chem. B*, **109**, 20072 (2005).
44. R. C. Mani, M. K. Sunkara, R. P. Baldwin, J. Gullapalli, J. A. Chaney, G. Bhimarasetti, J. M. Cowley, A. M. Rao, and R. Rao, *J. Electrochem. Soc.*, **152**, E154 (2005).
45. P. Ramesh and S. Sampath, *Electroanalysis*, **16**, 866 (2004).